

Numerically exact, time-dependent treatment of vibrationally coupled electron transport in single-molecule junctions

Haobin Wang

*Department of Chemistry and Biochemistry, MSC 3C,
New Mexico State University, Las Cruces, NM 88003*

Ivan Pshenichnyuk, Rainer Härtle, Michael Thoss

*Institut für Theoretische Physik und Interdisziplinäres Zentrum für Molekulare Materialien,
Friedrich-Alexander-Universität Erlangen-Nürnberg,
Staudtstr. 7/B2, D-91058, Germany*

Abstract

The multilayer multiconfiguration time-dependent Hartree (ML-MCTDH) theory within second quantization representation of the Fock space, a novel numerically exact methodology to treat many-body quantum dynamics for systems containing identical particles, is applied to study the effect of vibrational motion on electron transport in a generic model for single-molecule junctions. The results demonstrate the importance of electronic-vibrational coupling for the transport characteristics. For situations where the energy of the bridge state is located close to the Fermi energy, the simulations show the time-dependent formation of a polaron state that results in a pronounced suppression of the current corresponding to the phenomenon of phonon blockade. We show that this phenomenon cannot be explained solely by the polaron shift of the energy but requires methods that incorporate the dynamical effect of the vibrations on the transport. The accurate results obtained with the ML-MCTDH in this parameter regime are compared to results of nonequilibrium Green's function (NEGF) theory.

I. INTRODUCTION

Charge transport in single-molecule junctions, i.e. single-molecules that are bound to metal or semiconductor electrodes, has been of great interest recently.¹⁻¹⁰ Employing different experimental techniques, including electromigration or mechanically controllable break junctions or scanning tunneling microscopy,^{1,11-28} the conductance properties of nanoscale molecular junctions have been investigated. The observed current-voltage characteristics typically exhibit a nonlinear behavior with resonance structures at larger bias voltages associated with the discrete energy levels of the molecular bridge. The experiments have also revealed a wealth of interesting transport phenomena including Coulomb blockade,¹³ the Kondo effect,²⁹ negative differential resistance,^{26,30,31} switching and hysteresis.³²⁻³⁴ Furthermore the possibility to obtain transport characteristics that resemble those of a diode²⁰ or a transistor¹¹ has been demonstrated. These findings have stimulated great interest in the basic mechanisms which govern quantum transport at the molecular scale.

An interesting aspect that distinguishes single-molecule junctions from mesoscopic devices is the influence of nuclear motion on electron transport. Because of the small size of molecules, the charging of the molecular bridge is often accompanied by significant changes of the nuclear geometry that result in strong coupling between electronic and vibrational degrees of freedom. This coupling may give rise to substantial current-induced vibrational excitation and thus may cause heating and possible breakage of the molecular junction. The signature of nuclear motion has been observed in conduction measurements of a variety of molecular junctions,^{11,14,16,18,19,25-27,35-46} e.g., H₂ between platinum electrodes,¹⁴ C₆₀ molecules between gold electrodes,¹¹ and copper phthalocyanine¹⁹ on aluminum oxide film. Vibrational signatures of molecular bridges have also been observed in inelastic electron tunneling spectroscopy.³⁵⁻³⁷ New experimental techniques⁴⁷⁻⁴⁹ based, e.g., on Raman spectroscopy, allow the characterization of the nonequilibrium state of the vibrational degrees of freedom in a molecular junction.

The experimental progress has stimulated much interest in the theoretical modeling and simulation of vibrationally coupled electron transport in molecular junctions. To this end, a variety of theoretical approaches have been developed and employed, including scattering theory,⁵⁰⁻⁵⁷ nonequilibrium Green's function approaches,⁵⁸⁻⁶⁶ and master equation methods.^{58,67-78} Although much physical insight has been obtained by the application of

these methods, all these approaches involve significant approximations. For example, NEGF methods and master equation approaches are usually based on (self-consistent) perturbation theory and/or employ factorization schemes. Scattering theory approaches to vibrationally coupled electron transport, on the other hand, neglect vibrational nonequilibrium effects and are limited to the treatment of a small number of vibrational degrees of freedom. Furthermore, a systematic improvement of these approaches to yield numerically exact result, though formally possible by, e.g., including higher orders in the perturbation expansion, is practically very challenging. These shortcomings have motivated us to develop a systematic, numerically exact methodology to study quantum dynamics and quantum transport including many-body effects, in particular, correlated electronic-nuclear dynamics — the multilayer multiconfiguration time-dependent Hartree (ML-MCTDH) theory in second quantization representation (SQR).⁷⁹ Other efforts along the same direction include the numerical path integral approach,^{80–82} real-time quantum Monte Carlo simulations,^{83,84} the numerical renormalization group approach,⁸⁵ and the time-dependent density matrix renormalization group.⁸⁶ For a comparison and an overview of various different methods in the related problem of nonequilibrium transport with electron-electron interaction see Ref. 87.

In this paper, we report results of accurate quantum simulations employing the ML-MCTDH-SQR theory for a generic model of vibrationally coupled electron transport through molecular junctions. The paper is organized as follows. Section II outlines the physical model and the observables of interest. The ML-MCTDH-SQR theory is described in Section III. Section IV presents numerical results for vibrationally coupled electron transport in different parameter regimes as well as an analysis of the transport mechanism. Moreover, the validity of NEGF theory in the regime of phonon blockade is discussed. Finally, Section V concludes.

II. MODEL AND OBSERVABLES OF INTEREST

To study vibrationally coupled electron transport we consider a simple generic model for a single-molecule junction. It comprises one discrete electronic state at the molecular junction, two electronic continua describing the left and the right metal leads, respectively, and a distribution of harmonic oscillators that models the vibrational modes of the molecular bridge. The Hamiltonian reads

$$\hat{H} = \hat{H}_{\text{el}} + \hat{H}_{\text{nuc}} + \hat{H}_{\text{el-nuc}}, \quad (2.1a)$$

where \hat{H}_{el} , \hat{H}_{nuc} , and $\hat{H}_{\text{el-nuc}}$ describe the electronic degrees of freedom, the nuclear vibrations, and their coupling terms, respectively

$$\begin{aligned} \hat{H}_{\text{el}} = & E_d d^\dagger d + \sum_{k_L} E_{k_L} c_{k_L}^\dagger c_{k_L} + \sum_{k_R} E_{k_R} c_{k_R}^\dagger c_{k_R} \\ & + \sum_{k_L} V_{dk_L} (d^\dagger c_{k_L} + c_{k_L}^\dagger d) + \sum_{k_R} V_{dk_R} (d^\dagger c_{k_R} + c_{k_R}^\dagger d), \end{aligned} \quad (2.1b)$$

$$\hat{H}_{\text{nuc}} = \frac{1}{2} \sum_j (P_j^2 + \omega_j^2 Q_j^2), \quad (2.1c)$$

$$\hat{H}_{\text{el-nuc}} = d^\dagger d \sum_j c_j Q_j. \quad (2.1d)$$

Thereby, d^\dagger/d , $c_{k_L}^\dagger/c_{k_L}$, $c_{k_R}^\dagger/c_{k_R}$ are the fermionic creation/annihilation operators for the electronic states on the molecular bridge, the left and the right leads, respectively. The corresponding electronic energies E_{k_L} , E_{k_R} and the molecule-lead coupling strengths V_{dk_L} , V_{dk_R} , are defined through the energy-dependent level width functions

$$\Gamma_L(E) = 2\pi \sum_{k_l} |V_{dk_L}|^2 \delta(E - E_{k_L}), \quad \Gamma_R(E) = 2\pi \sum_{k_r} |V_{dk_R}|^2 \delta(E - E_{k_R}). \quad (2.2)$$

In principle, the parameters of the model can be obtained for a specific molecular junction employing first-principles electronic structure calculations.⁸⁸ In this paper, which focuses on the transport methodology, however, we will use a generic parametrization. Employing a tight-binding model, the function $\Gamma(E)$ is given as

$$\Gamma(E) = \begin{cases} \frac{\alpha_e^2}{\beta_e^2} \sqrt{4\beta_e^2 - E^2} & |E| \leq 2|\beta_e| \\ 0 & |E| > 2|\beta_e| \end{cases}, \quad (2.3a)$$

$$\Gamma_L(E) = \Gamma(E - \mu_L), \quad \Gamma_R(E) = \Gamma(E - \mu_R), \quad (2.3b)$$

where β_e and α_e are nearest-neighbor couplings between two lead sites and between the lead and the bridge state, respectively. I.e., the width functions for the left and the right leads are obtained by shifting $\Gamma(E)$ relative to the chemical potentials of the corresponding leads. We consider a simple case of two identical leads, in which the chemical potentials are given by

$$\mu_{L/R} = E_f \pm V/2, \quad (2.4)$$

where V is the bias voltage and E_f the Fermi energy of the leads. Since only the difference $E_d - E_f$ is physically relevant, we set $E_f = 0$ in this paper.

The frequencies ω_j and electronic-nuclear coupling constants c_j of the vibrational modes of the molecular junctions are modeled by a spectral density function^{89,90}

$$J(\omega) = \frac{\pi}{2} \sum_j \frac{c_j^2}{\omega_j} \delta(\omega - \omega_j). \quad (2.5)$$

In this paper, the spectral density is chosen in Ohmic form with an exponential cutoff

$$J_O(\omega) = \frac{\pi}{2} \alpha \omega e^{-\omega/\omega_c}, \quad (2.6)$$

where α is the dimensionless Kondo parameter.

Both the electronic and the vibrational continua can be discretized using an appropriate scheme.⁹¹ Within a given time scale the numbers of electronic states and bath modes are systematically increased to reach converged results for the quantum dynamics in the condensed phase. In this paper, we employ 64-128 states for each electronic lead, implying 32-64 electrons per lead, and a bath with 100-400 modes.

The observable of interest in transport through molecular junctions is the current for a given bias voltage, given by (in this paper we use atomic units where $\hbar = e = 1$)

$$I_L(t) = -\frac{dN_L(t)}{dt} = -\frac{1}{\text{tr}[\hat{\rho}]} \text{tr} \left\{ \hat{\rho} e^{i\hat{H}t} i[\hat{H}, \hat{N}_L] e^{-i\hat{H}t} \right\}, \quad (2.7a)$$

$$I_R(t) = \frac{dN_R(t)}{dt} = \frac{1}{\text{tr}[\hat{\rho}]} \text{tr} \left\{ \hat{\rho} e^{i\hat{H}t} i[\hat{H}, \hat{N}_R] e^{-i\hat{H}t} \right\}. \quad (2.7b)$$

Here, $N_{L/R}(t)$ denotes the time-dependent charge in each lead, defined as

$$N_\zeta(t) = \frac{1}{\text{tr}[\hat{\rho}]} \text{tr}[\hat{\rho} e^{i\hat{H}t} \hat{N}_\zeta e^{-i\hat{H}t}], \quad \zeta = L, R. \quad (2.8)$$

In the expression above $\hat{N}_\zeta = \sum_{k_\zeta} c_{k_\zeta}^+ c_{k_\zeta}$ is the occupation number operator for the electrons in each lead ($\zeta = L, R$) and $\hat{\rho}$ is the initial density matrix representing a grand-canonical ensemble for each lead and a certain preparation for the bridge state

$$\hat{\rho} = \hat{\rho}_d^0 \exp \left[-\beta(\hat{H}_0 - \mu_L \hat{N}_L - \mu_R \hat{N}_R) \right], \quad (2.9a)$$

$$\hat{H}_0 = \sum_{k_l} E_{k_l} c_{k_l}^+ c_{k_l} + \sum_{k_r} E_{k_r} c_{k_r}^+ c_{k_r} + \hat{H}_{\text{nuc}}^0. \quad (2.9b)$$

Here $\hat{\rho}_d^0$ is the initial reduced density matrix for the bridge state, which is usually chosen as a pure state representing an occupied or an empty bridge state, and \hat{H}_{nuc}^0 defines the initial bath equilibrium distribution, e.g., \hat{H}_{nuc} given above. The dependence of the steady-state

current on the initial density matrix is a complex issue and is partly addressed in the results section of this paper. Finally, for Hamiltonian (2.1) the explicit expression for the current operator is given as

$$\hat{I}_\zeta \equiv i[\hat{H}, \hat{N}_\zeta] = i \sum_{k_\zeta} V_{dk_\zeta} (d^+ c_{k_\zeta} - c_{k_\zeta}^+ d), \quad \zeta = L, R. \quad (2.10)$$

The transient behavior of the thus defined currents $I_R(t)$ and $I_L(t)$ is usually different. However, the long-time limits of $I_R(t)$ and $I_L(t)$, which define the stationary current, are the same. It is found that the average current

$$I(t) = \frac{1}{2}[I_R(t) + I_L(t)], \quad (2.11)$$

provides better numerical convergence properties by minimizing the transient characteristic, and thus will be used in this paper.

Within the model, the left and right leads represent the electronic continuum, each containing an infinite number of states. As mentioned above, in our simulations this continuous distribution is represented by a finite number of electronic states. The number of states required to properly describe the continuum limit depends on the time t . The situation is thus similar to that of a quantum reactive scattering calculation in the presence of a scattering continuum, where, with a finite number of basis functions, an appropriate absorbing boundary condition is added to mimic the correct outgoing Green's function.⁹²⁻⁹⁵ Employing the same strategy for the present problem, the regularized electric current is given by

$$I^{\text{reg}} = \lim_{\eta \rightarrow 0^+} \int_0^\infty dt \frac{dI(t)}{dt} e^{-\eta t}. \quad (2.12)$$

The regularization parameter η is similar (though not identical) to the formal convergence parameter in the definition of the Green's function in terms of the time evolution operator

$$G(E^+) = \lim_{\eta \rightarrow 0^+} (-i) \int_0^\infty dt e^{i(E+i\eta-H)t}. \quad (2.13)$$

In numerical calculations, η is chosen in a similar way as the absorbing potential used in quantum scattering calculations.⁹²⁻⁹⁵ In particular, the parameter η has to be large enough to accelerate the convergence but still sufficiently small in order not to affect the correct result. While in the reactive scattering calculation η is often chosen to be coordinate dependent, in our simulation η is chosen to be time dependent

$$\eta(t) = \begin{cases} 0 & (t < \tau) \\ \eta_0 \cdot (t - \tau)/t & (t > \tau). \end{cases} \quad (2.14)$$

Here η_0 is a damping constant, τ is a cutoff time beyond which a steady state charge flow is approximately reached. As the number of electronic states increases, one may choose a weaker damping strength η_0 and/or longer cutoff time τ . The former approaches zero and the latter approaches infinity for an infinite number of states. In practice, for the systems considered in this work, convergence can be reached with a reasonable number of electronic states in the range of 64-128, with a typical $\tau = 40-60$ fs (a smaller τ for less number of states) and $1/\eta_0 = 2-5$ fs.

To analyze the transport mechanisms, it is also expedient to consider the population of the electronic state localized on the the molecular bridge, which is given by

$$P_d(t) = \frac{1}{\text{tr}[\hat{\rho}]} \text{tr} \left\{ \hat{\rho} e^{i\hat{H}t} d^+ d e^{-i\hat{H}t} \right\}. \quad (2.15)$$

III. THE MULTILAYER MULTICONFIGURATION TIME-DEPENDENT HARTREE THEORY IN SECOND QUANTIZATION REPRESENTATION

The accurate treatment of the time-dependent transport problem outlined above requires a method that is able to describe the quantum dynamics of a system with many electronic and nuclear degrees of freedom. To this end, we employ the recently proposed Multilayer Multiconfiguration Time-Dependent Hartree Theory in Second Quantization Representation (ML-MCTDH-SQR).⁹⁶ This method extends the ML-MCTDH approach to the treatment of indistinguishable particles.

A. General formulation of the ML-MCTDH theory

The ML-MCTDH theory⁹¹ is a rigorous variational method to propagate wave packets in complex systems with many degrees of freedom. In this approach the wave function is represented by a recursive, layered expansion,

$$|\Psi(t)\rangle = \sum_{j_1} \sum_{j_2} \dots \sum_{j_p} A_{j_1 j_2 \dots j_p}(t) \prod_{\kappa=1}^p |\varphi_{j_\kappa}^{(\kappa)}(t)\rangle, \quad (3.1a)$$

$$|\varphi_{j_\kappa}^{(\kappa)}(t)\rangle = \sum_{i_1} \sum_{i_2} \dots \sum_{i_{Q(\kappa)}} B_{i_1 i_2 \dots i_{Q(\kappa)}}^{\kappa, j_\kappa}(t) \prod_{q=1}^{Q(\kappa)} |v_{i_q}^{(\kappa, q)}(t)\rangle, \quad (3.1b)$$

$$|v_{i_q}^{(\kappa,q)}(t)\rangle = \sum_{\alpha_1} \sum_{\alpha_2} \dots \sum_{\alpha_{M(\kappa,q)}} C_{\alpha_1 \alpha_2 \dots \alpha_{M(\kappa,q)}}^{\kappa,q,i_q}(t) \prod_{\gamma=1}^{M(\kappa,q)} |\xi_{\alpha_\gamma}^{\kappa,q,\gamma}(t)\rangle, \quad (3.1c)$$

where $A_{j_1 j_2 \dots j_p}(t)$, $B_{i_1 i_2 \dots i_{Q(\kappa)}}^{\kappa,j_\kappa}(t)$, $C_{\alpha_1 \alpha_2 \dots \alpha_{M(\kappa,q)}}^{\kappa,q,i_q}(t)$ and so on are the expansion coefficients for the first, second, third, ..., layers, respectively; $|\varphi_{j_\kappa}^{(\kappa)}(t)\rangle$, $|v_{i_q}^{(\kappa,q)}(t)\rangle$, $|\xi_{\alpha_\gamma}^{\kappa,q,\gamma}(t)\rangle$, ..., are the “single particle” functions (SPFs) for the first, second, third, ..., layers. In Eq. (3.1a), p denotes the number of single particle (SP) groups/subspaces for the first layer. Similarly, $Q(\kappa)$ in Eq. (3.1b) is the number of SP groups for the second layer that belongs to the κ th SP group in the first layer, i.e., there are a total of $\sum_{\kappa=1}^p Q(\kappa)$ second layer SP groups. Continuing along the multilayer hierarchy, $M(\kappa, q)$ in Eq. (3.1c) is the number of SP groups for the third layer that belongs to the q th SP group of the second layer and the κ th SP group of the first layer, resulting in a total of $\sum_{\kappa=1}^p \sum_{q=1}^{Q(\kappa)} M(\kappa, q)$ third layer SP groups. Naturally, the size of the system that the ML-MCTDH theory can treat increases with the number of layers in the expansion. In principle, such a recursive expansion can be carried out to an arbitrary number of layers. The multilayer hierarchy is terminated at a particular level by expanding the SPFs in the deepest layer in terms of time-independent configurations, each of which may contain several Cartesian degrees of freedom.

The variational parameters within the ML-MCTDH theoretical framework are dynamically optimized through the use of Dirac-Frenkel variational principle⁹⁷

$$\langle \delta\Psi(t) | i \frac{\partial}{\partial t} - \hat{H} | \Psi(t) \rangle = 0, \quad (3.2)$$

which results in a set of coupled, nonlinear differential equations

$$i|\dot{\Psi}(t)\rangle_{\text{L1 coefficients}} = \hat{H}(t)|\Psi(t)\rangle, \quad (3.3a)$$

$$i|\dot{\underline{\varphi}}^{\kappa}(t)\rangle_{\text{L2 coefficients}} = [1 - \hat{P}^{(\kappa)}(t)][\hat{\rho}^{(\kappa)}(t)]^{-1} \langle \hat{H} \rangle^{(\kappa)}(t) |\underline{\varphi}^{\kappa}(t)\rangle, \quad (3.3b)$$

$$i|\dot{\underline{v}}^{(\kappa,q)}(t)\rangle_{\text{L3 coefficients}} = [1 - \hat{P}_{\text{L2}}^{(\kappa,q)}(t)][\hat{\rho}_{\text{L2}}^{(\kappa,q)}(t)]^{-1} \langle \hat{\mathcal{H}} \rangle_{\text{L2}}^{(\kappa,q)}(t) |\underline{v}^{(\kappa,q)}(t)\rangle, \quad (3.3c)$$

$$i|\dot{\underline{\xi}}^{(\kappa,q,\gamma)}(t)\rangle_{\text{L4 coefficients}} = [1 - \hat{P}_{\text{L3}}^{(\kappa,q,\gamma)}(t)][\hat{\rho}_{\text{L3}}^{(\kappa,q,\gamma)}(t)]^{-1} \langle \hat{\mathcal{H}} \rangle_{\text{L3}}^{(\kappa,q,\gamma)}(t) |\underline{\xi}^{(\kappa,q,\gamma)}(t)\rangle, \quad (3.3d)$$

...

For referencing purpose we label the SP subspaces from top to bottom layers as level one (L1), level 2 (L2), and so on. In the notation used in Eq. (3.3) the time derivatives on the left

hand side (represented by a dot) are only performed with respect to the expansion coefficients of a particular layer (denoted by the respective subscript). For example, the time derivative in Eq. (3.3a) acts only on the L1 expansion coefficient $A_{j_1 j_2 \dots j_p}(t)$; the time derivative in Eq. (3.3b) is on the L2 expansion coefficient $B_{i_1 i_2 \dots i_{Q(\kappa)}}^{\kappa, j_\kappa}(t)$; etc. In our convention, for a N -layer version of the ML-MCTDH theory there are $N + 1$ levels of expansion coefficients. In this sense the conventional wave packet propagation method is a “zero-layer” MCTDH approach.

In practical implementations various intermediate quantities are defined within the subspaces of each layer of the wave function.⁹¹ For example, the top-layer Hamiltonian matrix $[\hat{H}(t)]_{JL} \equiv \langle \Phi_J(t) | \hat{H} | \Phi_L(t) \rangle$, where $|\Phi_J(t)\rangle \equiv \prod_{\kappa=1}^p |\varphi_{j_\kappa}^{(\kappa)}(t)\rangle$ is a configuration in the L1 subspace; the reduced density matrices $\hat{\rho}^{(\kappa)}(t)$, $\hat{\rho}_{L2}^{(\kappa, q)}(t)$, $\hat{\rho}_{L3}^{(\kappa, q, \gamma)}(t)$, ..., $\hat{\rho}_{LN}^{(\kappa, q, \gamma, \dots)}(t)$ for the first, second, third, and Nth layers, respectively; and the corresponding mean-field operators $\langle \hat{H} \rangle^{(\kappa)}(t)$, $\langle \hat{\mathcal{H}} \rangle_{L2}^{(\kappa, q)}(t)$, $\langle \hat{\mathcal{H}} \rangle_{L3}^{(\kappa, q, \gamma)}(t)$, ..., $\langle \hat{\mathcal{H}} \rangle_{LN}^{(\kappa, q, \gamma, \dots)}(t)$. These operators can be recursively evaluated by means of the single hole functions $|\Psi_m^{(\kappa)}(t)\rangle$, $|g_{L2; m, s}^{(\kappa, q)}(t)\rangle$, $|g_{L3; m, s}^{(\kappa, q, \gamma)}(t)\rangle$, ..., for the first, second, third, and further layers.^{79,91,96}

The introduction of this recursive, dynamically optimized layering scheme in the ML-MCTDH wavefunction provides more flexibility in the variational functional, which results in tremendous gain in our ability to study large quantum many-body systems. During the past few years, significant progress has been made in further development of the theory to simulate quantum dynamics and nonlinear spectroscopy of ultrafast electron transfer reactions in condensed phases.^{96,98–108} The theory has also been generalized to study heat transfer through molecular junctions¹⁰⁹ and to calculate rate constants for model proton transfer reactions in molecules in solution.^{110,111} Recent work of Manthe has introduced an even more adaptive formulation based on a layered correlation discrete variable representation (CDVR).^{112,113}

B. Treating identical particles using the second quantization representation of Fock space

Despite its previous success, the original ML-MCTDH theory was not directly applicable to studying systems of identical quantum particles. This is because an ordinary Hartree product in the first quantized picture is only suitable to describe a configuration for a

system of distinguishable particles. To handle systems of identical particles, one strategy is to employ a properly symmetrized wave function, i.e., permanents in a bosonic case or Slater determinants in a fermionic case. This led to the MCTDHF approach^{114–116} for treating identical fermions and the MCTDHB approach¹¹⁷ for treating identical bosons as well as combinations thereof.¹¹⁸ However, this wave function-based symmetrization is only applicable to the single layer MCTDH theory but is incompatible with the ML-MCTDH theory with more layers — there is no obvious analog of a multilayer Hartree configuration if permanents/determinants are used to represent the wave function. As a result, the ability to treat much larger quantum systems numerically exactly was severely limited.

To overcome this limitation we proposed a novel approach⁷⁹ that follows a fundamentally different route to tackle quantum dynamics of indistinguishable particles — an operator-based method that employs the second quantization formalism of many-particle quantum theory. Thereby the variation is carried out entirely in the abstract Fock space using the occupation number representation. This differs from many previous methods where the second quantization formalism is only used as a convenient tool to derive intermediate expressions for the first quantized form. In the new approach the burden of handling symmetries of identical particles in a numerical variational calculation is shifted completely from wave functions to the algebraic properties of operators.

The procedure can be illustrated by considering a system of identical fermions. In the first quantized representation a Slater determinant $|\chi_{P_1}\chi_{P_2}\dots\chi_{P_N}\rangle$ describes an anti-symmetric N -particle state by choosing N spin orbitals out of the M orthonormal spin-adapted basis functions, $\{\chi_1(\mathbf{x}), \chi_2(\mathbf{x}), \dots, \chi_M(\mathbf{x})\}$. All possible Slater determinants in this form constitute the fermionic subspace of the N -particle Hilbert space, denoted by $\mathcal{H}(M, N)$. The Fock space $\mathcal{F}(M)$ is formed by considering an arbitrary number of particles

$$\mathcal{F}(M) = \mathcal{H}(M, 0) \oplus \mathcal{H}(M, 1) \oplus \mathcal{H}(M, 2) \oplus \dots \oplus \mathcal{H}(M, M). \quad (3.4)$$

In second quantization a convenient basis to represent the Fock space is the occupation number basis

$$|\mathbf{n}\rangle \equiv |n_1, n_2, \dots, n_M\rangle, \quad (3.5)$$

where n_P can be either 1 if the one-particle state χ_P is occupied [i.e., present in the original Slater determinant] or 0 if it is unoccupied. The number of particles in state $|\mathbf{n}\rangle$ is given by $N = \sum_{P=1}^M n_P$, and thus $\mathcal{H}(M, N)$ contains all occupation-number vectors with N particles.

Each occupation-number state is defined by acting a series of creation operators a_P^\dagger on the vacuum state, $|\mathbf{n}\rangle = \prod_{P=1}^M (a_P^\dagger)^{n_P} |\text{vac}\rangle$.

In contrast to a Slater determinant, the occupation-number state $|\mathbf{n}\rangle$ can be formally written in the form of a Hartree product,¹¹⁹

$$|\mathbf{n}\rangle = \prod_{P=1}^M |n_P\rangle \equiv |n_1\rangle |n_2\rangle \dots |n_M\rangle. \quad (3.6)$$

This formal factorization suggests a different decomposition of the Fock space

$$\mathcal{F}(M) = f_1(1) \otimes f_2(1) \otimes \dots \otimes f_\kappa(1) \otimes \dots \otimes f_M(1), \quad (3.7a)$$

where $f_\kappa(1)$ represents a single spin-orbital subspace with two possibilities/states: occupied or unoccupied. Bigger subspaces can be formed by grouping a few spin orbitals together

$$\mathcal{F}(M) = f_1(m_1) \otimes f_2(m_2) \otimes \dots \otimes f_\kappa(m_\kappa) \otimes \dots \otimes f_L(m_L), \quad M = \sum_{\kappa=1}^L m_\kappa, \quad (3.7b)$$

where $f_\kappa(m_\kappa)$ represents the subspace with m_κ spin orbitals and thus 2^{m_κ} states.

The decomposition schemes in Eqs. (3.7a) and (3.7b) are conceptually different from that in (3.4). They no longer require dealing with a full-length occupation-number vector in one step and treating it as a whole, unbreakable object like the original Slater determinant, but rather focus on each subspace $f_\kappa(m_\kappa)$ containing 2^{m_κ} linearly independent sub-vectors $\{\phi_{I_\kappa}^{(\kappa)}\}$, $I_\kappa = 1, \dots, 2^{m_\kappa}$. The crucial point is that in a variational calculation each sub-vector in the κ th subspace is not restricted to a particular fixed basis vector $\{\phi_{I_\kappa}^{(\kappa)}\}$, but may also be an appropriate superposition of all the sub-vectors in this subspace. One may then express the overall wave function in the same multilayer form as in Eq. (3.1). Take, for example, three explicit layers in (3.1), the deepest layer (3rd layer here) is expanded in the full basis sub-vectors in the Fock subspace as,

$$|\xi_{\alpha_\gamma}^{\kappa,q,\gamma}(t)\rangle = \sum_{n_1=0}^1 \sum_{n_2=0}^1 \dots \sum_{n_{m(\kappa,q,\gamma)}=0}^1 D_{n_1 n_2 \dots n_{m(\kappa,q,\gamma)}}^{\kappa,q,\gamma,\alpha_\gamma}(t) |n_1\rangle |n_2\rangle \dots |n_{m(\kappa,q,\gamma)}\rangle. \quad (3.8)$$

$|\Psi(t)\rangle$ in Eq. (3.1) is then built “bottom-up” from the optimal, time-dependent SPFs for the subspaces.

After introducing the occupation-number representation of the Fock space, the Hamiltonian can be expressed in terms of fermionic creation/annihilation operators via the standard procedure in the second quantization formalism.^{120,121} The overall method is thus a

ML-MCTDH theory in second quantization representation (SQR). The major difference between the ML-MCTDH-SQR theory for identical fermions and the previous ML-MCTDH theory for distinguishable particles is the way how operators act. In the second quantized form the fermionic creation/annihilation operators fulfill the anti-commutation relations

$$\{a_P, a_Q^+\} \equiv a_P a_Q^+ + a_Q^+ a_P = \delta_{PQ}, \quad \{a_P^+, a_Q^+\} = \{a_P, a_Q\} = 0. \quad (3.9)$$

The symmetry of identical particles is thus realized by enforcing such algebraic properties of the operators.

The practical procedure can be illustrated by considering a single layer theory in the form of Eq. (3.7b), where each SP group κ corresponds to a Fock subspace in (3.7b)

$$|\Psi(t)\rangle = \sum_{j_1} \sum_{j_2} \dots \sum_{j_L} A_{j_1 j_2 \dots j_L}(t) \prod_{\kappa=1}^L |\varphi_{j_\kappa}^{(\kappa)}(t)\rangle, \quad (3.10a)$$

$$|\varphi_{j_\kappa}^{(\kappa)}(t)\rangle = \sum_{I_\kappa=1}^{2^{m_\kappa}} B_{I_\kappa}^{\kappa, j_\kappa}(t) |\phi_{I_\kappa}^{(\kappa)}\rangle \equiv \sum_{n_1=0}^1 \sum_{n_2=0}^1 \dots \sum_{n_{m_\kappa}=0}^1 B_{n_1 n_2 \dots n_{m_\kappa}}^{\kappa, j_\kappa}(t) |n_1\rangle |n_2\rangle \dots |n_{m_\kappa}\rangle. \quad (3.10b)$$

Without loss of generality let us consider acting a creation operator $(a_\nu^{(\kappa)})^+$ on the SPFs. In practical implementation this operation is equivalent to

$$(a_\nu^{(\kappa)})^+ = \left(\prod_{\mu=1}^{\kappa-1} \hat{S}_\mu \right) (\tilde{a}_\nu^{(\kappa)})^+, \quad (3.11)$$

where \hat{S}_μ ($\mu = 1, 2, \dots, \kappa - 1$) is the permutation sign operator that accounts for permuting $(a_\nu^{(\kappa)})^+$ from the first subspace all the way through to the κ th subspace, and $(\tilde{a}_\nu^{(\kappa)})^+$ is the reduced creation operator that only takes care of the fermionic anti-commutation relation in the κ th subspace. The operator-based anti-commutation constraint (3.9) results in the following operations

$$(\tilde{a}_\nu^{(\kappa)})^+ |\varphi_{j_\kappa}^{(\kappa)}(t)\rangle = \sum_{n_1=0}^1 \sum_{n_2=0}^1 \dots \sum_{n_{m_\kappa}=0}^1 \delta_{n_\nu, 0} \left[\prod_{q=1}^{\nu-1} (-1)^{n_q} \right] B_{n_1 n_2 \dots n_{m_\kappa}}^{\kappa, j_\kappa}(t) |n_1\rangle |n_2\rangle \dots |1_\nu\rangle \dots |n_{m_\kappa}\rangle, \quad (3.12a)$$

$$\hat{S}_\mu |\varphi_{j_\mu}^{(\mu)}(t)\rangle = \sum_{n_1=0}^1 \sum_{n_2=0}^1 \dots \sum_{n_{m_\mu}=0}^1 \left[\prod_{q=1}^{m_\mu} (-1)^{n_q} \right] B_{n_1 n_2 \dots n_{m_\mu}}^{\mu, j_\mu}(t) |n_1\rangle |n_2\rangle \dots |n_{m_\mu}\rangle. \quad (3.12b)$$

I.e., $(\tilde{a}_\nu^{(\kappa)})^+$ not only creates a particle in the ν th spin orbital if it is vacant, but also affects the sign of each term in this SPF according to where ν is located and what the occupations are prior to it. Furthermore, the permutation sign operators \hat{S}_μ , $\mu = 1, 2, \dots, \kappa - 1$, incorporate

the sign changes of the remaining spin orbitals in all the SPFs whose subspaces are prior to that of $(\tilde{a}_\nu^{(\kappa)})^+$.

The implementation of Eq. (3.11) is sophisticated but nevertheless a routine practice in the MCTDH or ML-MCTDH theory — a product of operators. Thereby, the action of each Hamiltonian term (product of creation/annihilation operators) can be split into a series of operations on individual Fock subspaces.

The generalization from the single layer to the multilayer case is tedious but straightforward. The Fock space is decomposed in a recursive, layered fashion — the spin orbitals here in the ML-MCTDH-SQR theory are treated in the same way as the degrees of freedom in the original ML-MCTDH theory, except that the orderings of all the SP groups in all layers need to be recorded and maintained in later manipulations. The wave function can then be recursively expanded via Eq. (3.1). More importantly, the equations of motion have the same form as in the original ML-MCTDH theory. The only difference is that each creation/annihilation operator of the Hamiltonian is effectively a product of operators: a reduced creation/annihilation operator that only acts on the bottom-layer SPFs for the Fock subspace it belongs to, and a series of permutation sign operators that accounts for the fermionic anti-commutation relations of all the spin orbitals prior to it.

In the second quantized form, the wave function is represented in the abstract Fock space employing the occupation number basis. As a result, it can be expanded in the same multilayer form as that for systems of distinguishable particles. It is thus possible to extend the numerically exact treatment to much larger systems. The symmetry of the wave function in the first quantized form is shifted to the operator algebra in the second quantized form. The key point is that, for both phenomenological models and more fundamental theories, there are only a limited number of combination of fundamental operators. For example, in electronic structure theory only one- and two-electron operators are present. This means that one never needs to handle all, redundant possibilities of operator combinations as offered by the determinant form in the first quantized framework. It is exactly this property that provides the flexibility of representing the wave functions in multilayer form and treat them accurately and efficiently within the ML-MCTDH-SQR theory. It is also noted that the ML-MCTDH-SQR approach outlined above for fermions has also be formulated for bosons or combinations of fermions, bosons and distinguishable particles.⁷⁹ Here, we apply it to vibrationally coupled electron transport, which involves a combination of vibrational

degrees of freedom and indistinguishable electrons.

IV. RESULTS AND DISCUSSION

In this section we present applications of the ML-MCTDH-SQR methodology to vibrationally coupled electron transport employing the model described in Sec. II. We first consider a model with the following set of electronic parameters: The energy of the discrete state E_d is located 0.5 eV above the Fermi energy of the leads ($E_f = 0$). The tight-binding parameters for the function $\Gamma(E)$ are $\alpha_e = 0.2$ eV, $\beta_e = 1$ eV, corresponding to a moderate molecule-lead coupling and a bandwidth of 4 eV.

Figure 1 shows the time-dependent current for low bias voltage, $V = 0.2$ V, and a range of different temperatures, 0 - 300 K. Panel (a) depicts the purely electronic current obtained without coupling to the vibrational degrees of freedom ($\alpha = 0$). In this case significant electronic coherence is observed for the current $I(t)$ at short time, which decreases for longer time. A plateau of $I(t)$ is reached in relative short time (~ 30 fs), which demonstrates the feasibility of using a time-dependent approach to obtain the stationary current. In contrast to the transient characteristics, for the purely electronic problem considered in Fig. 1(a) the stationary current can also be obtained exactly from the Green's function or the scattering theory approach, employing e.g. Landauer theory.^{4,122,123} The thus obtained stationary value of the current agrees with the simulation result. The results in Fig. 1(a) also illustrate the fairly weak temperature dependence of $I(t)$ for this set of electronic parameters.

Figure 1(b) shows results for the same electronic parameters as in Fig. 1(a), however including the coupling to the vibrational bath. The characteristic frequency of the bath has been chosen as $\omega_c = 500$ cm⁻¹ and the overall electronic-nuclear coupling strength is determined by the reorganization energy, $\lambda = 2\alpha\omega_c = 2000$ cm⁻¹. These parameters represent typical values for polyatomic molecules.⁵⁰ It is noted that in contrast to many previous treatments of vibrationally coupled electron transport in molecular junctions, the present method allows a nonperturbative, in principle numerically exact treatment of this nonequilibrium problem. The results show that the inclusion of electronic-vibrational coupling has a significant effect on the transport characteristics. In particular, it causes a quenching of the electronic coherence. As a result, the time scale on which the current $I(t)$ reaches its stationary value is shorter. Furthermore, the temperature dependence of the current is

more pronounced than in the corresponding purely electronic case. It is also noted that in this particular physical regime the value of the current is larger than for purely electronic transport (*vide infra*).

Figure 2 shows the time-dependent current for different electronic-vibrational coupling strengths. While smaller electronic-vibrational coupling ($\lambda \leq 1000 \text{ cm}^{-1}$) causes mostly decoherence in the transient regime, larger coupling is seen to influence also the stationary value of the current significantly. This can be understood qualitatively from the fact that the coupling to the vibrations effectively lowers the energy level of the bridge (polaron shift). For the given voltage, the bare energy of the electronic bridge state is still outside the conductance window, which is defined by the chemical potentials of the two electrodes. The coupling to the vibrations brings the level closer to the chemical potential of the electrodes. As a result, the current is enhanced. The value of this polaron shift of the energy is given by the reorganization energy λ . For example, while for a value of $\lambda = 1000 \text{ cm}^{-1}$ the predominant transport mechanism is nonresonant tunneling, for a value of $\lambda = 4000 \text{ cm}^{-1}$ the polaron-shifted bridge state is already inside the conductance window between the chemical potential of the electrodes and thus the transport mechanism is resonant tunneling.

We next consider a model with the same parameters except that the energy of the bridge state is below the Fermi energy, $E_d - E_f = -0.5 \text{ eV}$. As shown in Figure 3, in this case an increase in the electronic-vibrational coupling strength not only quenches the electronic coherence but also reduces the current monotonically. This is due to the fact that if the bridge state is located below the Fermi levels of the leads (Figure 3) the coupling to the vibrational bath will shift its effective energy further away from the resonant transport regime. Note that, as implied by the model Hamiltonian, Eq. (2.1), the calculations depicted in Figure 3 use the same electronic reference state as for Figure 2, i.e. the polaron shift is to lower energies for both calculations. Figure 4 displays the current-voltage characteristics for the two models with the same electronic parameters as in Figs. 3 and 4, respectively, coupled to a bath with a characteristic frequency of $\omega_c = 500 \text{ cm}^{-1}$ and a reorganization energy of $\lambda = 2000 \text{ cm}^{-1}$. The simulation results are compared with the results for a purely electronic system obtained using the Landauer formula. The results show a pronounced influence of the vibrational coupling. In this particular parameter regime, for $E_d - E_f = 0.5 \text{ eV}$ the vibrationally coupled transport current is higher than that for the purely electronic model, whereas for $E_d - E_f = -0.5 \text{ eV}$ the situation is opposite. Although this can be

qualitatively explained by the polaron shift of the energy of the bridge state as discussed above, the actual quantitative prediction is more complex and requires a non-perturbative, accurate approach (*vide infra*).

It is worthwhile to point out that the initial condition used in the expression for the current, Eq. (2.9), is not unique. For example, one may choose an initially unoccupied bridge state and an unshifted bath of oscillators, i.e. H_{nuc} as given in Eq. (2.1). On the other hand, one may also start with a fully occupied bridge state and a bath of oscillators in equilibrium with the occupied bridge state

$$H'_{\text{nuc}} = \frac{1}{2} \sum_j \left[P_j^2 + \omega_j^2 \left(Q_j + \frac{c_j}{\omega_j^2} \right)^2 \right]. \quad (4.1)$$

Other initial states may also be prepared. Thus the question arises, whether the stationary current depends on the initial state that is used in the time-dependent simulation.

For the model parameters considered in this paper, our calculations show that the stationary state is independent on the initial condition. As an example, Figure 5(a) shows that the two initial states discussed above indeed give the same stationary current for the electronic parameters $\alpha_e = 0.2$ eV, $\beta_e = 1$ eV, $E_d - E_f = 0.5$ eV, $V = 0.1$ V, and the vibrational parameters $\lambda = 2000$ cm⁻¹ and $\omega_c = 500$ cm⁻¹, despite the fact that their initial transient characteristics are quite different. As illustrated in Figure 5(b), this is due to the fact that although the initial bridge state populations $P_d(t)$, defined by Eq. (2.15), are quite different, they attain the same stationary value within a relatively short time scale. For other parameters, however, the stationary state may depend on the initial condition. The investigation of the corresponding phenomenon of bistability^{124–129} will be the subject of future work.¹³⁰

We note that different sets of initial conditions also affect the time scale at which the current $I(t)$ reaches its stationary value, as is evident from Figure 5. In our simulations we typically choose initial conditions that are close to the final steady state, e.g., an unoccupied initial bridge state with an unshifted bath of oscillators for the transport calculations of Fig. 4(a) and an occupied bridge state with a bath of oscillators in equilibrium with the occupied bridge state for calculations of Fig. 4(b).

We finally consider a model where the energy of the bridge state is located at the Fermi energy of the leads. This parameter regime is particularly interesting, because already for small bias voltage the transport mechanism corresponds to resonant tunneling and involves

mixed electron/hole transport. For a purely electronic model, the Landauer formula predicts the maximum current when $E_d = E_f$. Including the couplings to the vibrational modes, however, may have a significant impact on the electric current. This is illustrated in Figure 6 for different electronic-vibrational coupling strengths λ . It is seen that for short time the current $I(t)$ obtained for finite λ follows the current for the purely electronic model ($\lambda = 0$). However, after a short transient time the coupling to the vibrations becomes effective and results in a suppression of the current. In particular for larger vibrational coupling, $\lambda = 2000 - 4000 \text{ cm}^{-1}$, the effect is very pronounced and the stationary current is essentially blocked over a significant range of bias voltages, as is demonstrated by the current-voltage characteristics in Figure 7.

The underlying mechanism can be qualitatively rationalized by considering the energy level of the bridge state. For any finite bias voltage, the bare energy of the bridge state ($E_d - E_f = 0$) is located between the chemical potential of the leads and thus, within a purely electronic model, current can flow. The coupling to the vibrations results in a polaron shift of the energy of the bridge state. For electronic-vibrational coupling strengths $\lambda > |V|/2$ the polaron-shifted energy of the bridge state is below the chemical potentials of both leads and thus current is blocked. This effect, referred to as phonon blockade of the current, has been observed e.g. in quantum dots.¹³¹

Although the interpretation of the phonon blockade in terms of the energetics of the bridge state is appealing, it should be emphasized that the mechanism of phonon blockade involves the formation of a many-body polaron-type state that is significantly more complex than this purely electronic picture and cannot be fully described by just considering the static shift of the energy of the bridge state. The bare energy and the polaron-shifted energy of the bridge state are only two special points on the multidimensional potential energy surface of the charged state given by $V_d(\mathbf{Q}) = E_d + \frac{1}{2} \sum_j \omega_j^2 Q_j^2 + \sum_j c_j Q_j$. For values $\lambda > |V|/2$ the potential energy surface of the discrete state crosses the chemical potential of the leads as a function of the nuclear coordinates Q_j . In this parameter regime, an accurate description of the vibrational dynamics and its coupling to the electronic degrees of freedom is required to obtain a quantitative description of the many-body polaron state and its transport characteristics. This is demonstrated in Figure 8, which compares the electric current obtained with a full vibrationally-coupled many-body ML-MCTDH-SQR calculation to that obtained with a purely electronic model for a polaron-shifted energy

of the bridge state, i.e. $E_d \rightarrow E_d - \lambda$. The comparison shows that the effect cannot be described properly with a purely electronic model but requires methods that incorporate the dynamical effect of the vibrations on the transport.

As discussed in the introduction, a variety of approximate methods have been developed and employed to describe vibrationally coupled electron transport in molecular junctions, including scattering theory,^{50–57} nonequilibrium Green’s function (NEGF) approaches,^{58–66} and master equation methods.^{58,67–78} However, only very few of them are applicable to the present model. This is because the model involves vibronic coupling to a relatively large number of vibrational modes in nonequilibrium. Master equation methods are limited to a small number of vibrational degrees of freedom that are treated in full nonequilibrium, while many scattering theory approaches neglect vibrational nonequilibrium effects. NEGF theory is, in principle, applicable to describe coupling to a larger number of harmonic vibrational modes in nonequilibrium. However, if implemented within the self-consistent Born approximation it is limited to small electron-vibrational coupling and has so far mostly been applied in the nonresonant tunneling regime.⁶⁶ To treat vibrationally coupled electron transport in the resonant regime, another NEGF method has been proposed by Galperin et al.⁵⁹ and extended by Härtle et al.^{61,62,132} Being based on the polaron transformation, this NEGF method is in principle able to treat moderate vibronic coupling strengths. We have applied this method to the present model employing 10 vibrational modes to model the vibrational distribution described by the spectral density, Eq. (2.6).¹³⁰ Fig. 9 shows a comparison of results of the NEGF method for the stationary current with those obtained from ML-MCTDH for different vibronic coupling strength. Overall, the results indicate that the NEGF method is capable of describing the suppression of the current due to phonon blockade. For small vibronic coupling the NEGF results are in almost quantitative agreement with the numerically exact results. However, for larger vibronic coupling NEGF theory underestimates the effect of phonon blockade. This is presumably due to the fact that the present model does not exhibit a strict time-scale separation between the electronic and nuclear degrees of freedom, which is a prerequisite for the NEGF method. These results demonstrate that with approximate methods the simulation of transport properties of the present model, which is in the nonperturbative regime, is challenging. A more general validation of the NEGF method in a broader regime requires extensive studies by both the ML-MCTDH-SQR and the NEGF methods and will be the subject of future work.

While the effect of phonon blockade of the stationary current is to be expected for energetic reasons, the treatment with the ML-MCTDH method also allows a detailed study of the time-dependent formation of the underlying many-body polaron state. For example, Figure 10 shows that the transient dynamics depends significantly on the characteristic frequency of the vibrational bath, ω_c , whereas the value of the stationary current is relatively insensitive to ω_c . This is due to the fact that the frequency ω_c determines the timescale on which the system moves on the potential energy surface from the initially prepared state, corresponding to the bare energy of the bridge states, to the relaxed state below the chemical potential of the leads.

It is worthwhile to emphasize that the mechanism of the phonon blockade analyzed here is different from that of the previously discussed Franck-Condon blockade,¹³³⁻¹³⁵ which also leads to a suppression of the current due to strong electronic-vibrational coupling. While the former can be removed by a gate potential that shifts the energy of the bridge state into the conductance window, i.e. between the chemical potential of the electrodes, the latter is rather insensitive to a gate potential.

We finally discuss some technical details of the numerical calculations employing the ML-MCTDH-SQR method. For the parameter regimes investigated in this paper, the stationary current is usually reached at approximately 20-60 fs. To ensure convergence most calculations were carried out to 100 fs. Within this time scale of simulation, 64-128 discrete states are used to represent each lead's electronic continuum, resulting in a total number of 64-128 electrons in the ML-MCTDH-SQR numerical treatment. The nuclear bath is represented by 100-400 modes. The converged number of basis functions for these vibrational modes ranges from a few to a few hundred. The calculation was performed with a four-layer ML-MCTDH-SQR theory, with one top-layer SP group for the vibrational modes and three top-layer SP groups for the electronic part. These SP groups are then recursively expanded via a binary tree (i.e., two lower-layer SP groups in each preceding upper-layer SP). The final converged results (to within 10% relative error) require 40-60 SPFs for each top-layer electronic SP group, 20-40 SPFs for all lower-layer electronic SPs, and 10 SPFs for all nuclear SP groups. This results in a total of $\sim 10^6$ equations to solve. Each simulation took between 20 hours and several days of CPU time on a typical personal computer. Calculations for a finite temperature bath requires ensemble average over a few hundred initial wave functions, and were performed on a Cray XT4 parallel computer.

The convergence of the ML-MCTDH-SQR simulation is illustrated in Figure 11, where the physical parameters are the same as those in Fig. 1 except for a different voltage of 0.1V. The calculations are performed with a four-layer ML-MCTDH-SQR scheme. For simplicity the convergence is shown for the following three different categories. In Figure 11(a) there are 64 electronic states for each lead and 50 modes for the nuclear bath. The number of the single particle functions (SPFs) is 10 for each nuclear SP group (of each layer), and the number of the SPFs for each electronic SP group (of each layer) is set the same and varied. In Figure 11(b) there are 64 electronic states for each lead, with 40 SPFs for each electronic SP group. The number of bath modes is varied, with 10 SPFs for each SP group of each layer. In Figure 11(c) there are 50 bath modes, with 10 SPFs for each SP group. The number of electronic states for each lead is varied, with 40 SPFs for each SP group (of each layer).

First, we consider the convergence with respect to the number of SPFs. Fig. 11(a) shows that the electronic (fermionic) degrees of freedom require a relatively large number of SPFs to achieve convergence. The steady state current obtained with 20 SPFs differs approximately 20% from the converged value, although the short time transient dynamics agrees well with other results obtained with a larger number of SPFs. In this case convergence is reached when the number of SPFs exceeds 30 for the electronic degrees of freedom. For the nuclear degrees of freedom, tests have shown that results obtained with 6 or 8 SPFs are nearly identical to that obtained with 10 SPFs. Thus, although we used 10 SPFs in all the calculations, we believe a smaller number could be equally satisfactory.

Next, we check convergence with respect to the number of bath modes. Figure 11(b) shows that only small differences are found when the number of modes changes from 10 to 200. If one is only interested in the steady state current and not the finer details of the transient dynamics of $I(t)$, then a bath of 10 modes is sufficient as is used in our NEGF calculations. On the other hand, to represent the electronic continuum within the timescale of simulation, a sufficient number of electronic states are required. As shown in Fig. 11(c), 20 states per lead is inadequate for both the transient $I(t)$ or the steady state current. For the case of Fig. 11 convergence is achieved when the number of states per lead is greater than 40.

V. CONCLUDING REMARKS

In this paper we have employed the ML-MCTDH-SQR method to simulate vibrationally coupled electron transport through single-molecule junctions. The ML-MCTDH-SQR method allows an accurate, in principle numerically exact treatment of this many-body quantum transport problem. The results obtained for a generic model demonstrate the importance of electronic-vibrational coupling, which has a significant influence on the transport properties. For situations where the energy of the bridge state is located close to the Fermi energy, the simulations show the time-dependent formation of a polaron state that results in a pronounced suppression of the current corresponding to the phenomenon of phonon blockade. We have shown that this phenomenon cannot be explained solely by the polaron shift of the energy but requires methods that incorporate the dynamical effect of the vibrations on the transport.

While some of these results have been discussed previously based on approximate methods, the present methodology does not involve any systematic approximations and provides accurate benchmark results. It can thus also be used to test the validity of more approximate methods. As an example, we have discussed the validity of a NEGF method in the parameter regime of phonon blockade, demonstrating that accurate methods such as ML-MCTDH are necessary to study transport in the strong coupling regime. A more detailed study of the validity of approximate methods as well as the application of the methodology to investigate signatures of vibronic effects in experimental transport spectra, such as, e.g., inelastic electron tunneling spectroscopy, will be the subject of future work.

It is also emphasized that the time-dependent treatment employed in the ML-MCTDH-SQR method provides not only information on the steady state but also on the transient dynamics and can thus also be used to study the influence of time-dependent electrical fields, such as, e.g., ac gate fields or optical pulses on the transport process.

In the present study we have focused on the effect of electronic-vibrational coupling on transport in molecular junctions. Another important mechanism is electron-electron interaction. The extension of the ML-MCTDH-SQR to include explicit electron-electron interaction is currently under way. This may open the perspective to a comprehensive many-body treatment of nonequilibrium charge transport at the nanoscale.

Acknowledgments

This work has been supported by the National Science Foundation CHE-1012479 (HW) and the Deutsche Forschungsgemeinschaft (DFG) through a research grant and the Cluster of Excellence Munich Center of Advanced Photonics (MT), and used resources of the Leibniz Rechenzentrum München, the Rechenzentrum Erlangen (RRZE), and the National Energy Research Scientific Computing Center, which is supported by the Office of Science of the U.S. Department of Energy under Contract No. DE-AC02-05CH11231.

-
- ¹ M. Reed, C. Zhou, C. Muller, T. Burgin, and J. Tour, *Science* **278**, 252 (1997).
 - ² A. Nitzan and M. A. Ratner, *Science* **300**, 1384 (2003).
 - ³ C. Joachim, J. Gimzewski, and A. Aviram, *Nature (London)* **408**, 541 (2000).
 - ⁴ J. Cuevas and E. Scheer, *Molecular Electronics: An Introduction to Theory and Experiment* (World Scientific, Singapore, 2010).
 - ⁵ A. Nitzan, *Annu. Rev. Phys. Chem.* **52**, 681 (2001).
 - ⁶ G. Cuniberti, G. Fagas, and K. Richter, *Introducing Molecular Electronics* (Springer, Heidelberg, 2005).
 - ⁷ Y. Selzer and D. L. Allara, *Annu. Rev. Phys. Chem.* **57**, 593 (2006).
 - ⁸ F. Chen, J. Hihath, Z. Huang, X. Li, and N. Tao, *Annu. Rev. Phys. Chem.* **58**, 535 (2007).
 - ⁹ L. Venkataraman, J. E. Klare, C. Nuckolls, M. S. Hybertsen, and M. L. Steigerwald, *Nature* **442**, 904 (2006).
 - ¹⁰ M. Galperin, M. A. Ratner, A. Nitzan, and A. Troisi, *Science* **319**, 1056 (2008).
 - ¹¹ H. Park, J. Park, A. Lim, E. Anderson, A. Alivisatos, and P. McEuen, *Nature (London)* **407**, 57 (2000).
 - ¹² X. Cui, A. Primak, X. Zarate, J. Tomfohr, O. Sankey, A. Moore, T. Moore, D. Gust, G. Harris, and S. Lindsay, *Science* **294**, 571 (2001).
 - ¹³ J. Park, A. Pasupathy, J. Goldsmith, C. Chang, Y. Yaish, J. Petta, M. Rinkoski, J. Sethna, H. Abruna, P. McEuen, and D. Ralph, *Nature (London)* **417**, 722 (2002).
 - ¹⁴ R. Smit, Y. Noat, C. Untiedt, N. Lang, M. van Hemert, and J. van Ruitenbeek, *Nature (London)* **419**, 906 (2002).
 - ¹⁵ J. Reichert, R. Ochs, D. Beckmann, H. Weber, M. Mayor, and H. von Lohneysen, *Phys. Rev. Lett.* **88**, 176804 (2002).
 - ¹⁶ N. Zhitenev, H. Meng, and Z. Bao, *Phys. Rev. Lett.* **88**, 226801 (2002).
 - ¹⁷ B. Xu and N. Tao, *Science* **301**, 1221 (2003).
 - ¹⁸ X. Qiu, G. Nazin, and W. Ho, *Phys. Rev. Lett.* **92**, 206102 (2004).
 - ¹⁹ N. Liu, N. Pradhan, and W. Ho, *J. Chem. Phys.* **120**, 11371 (2004).
 - ²⁰ M. Elbing, R. Ochs, M. Koentopp, M. Fischer, C. von Hänisch, F. Weigend, F. Evers, H. Weber, and M. Mayor, *Proc. Natl. Acad. Sci. USA* **102**, 8815 (2005).

- ²¹ M. Elbing, R. Ochs, M. Koentopp, M. Fischer, C. von Hänisch, F. Weigend, F. Evers, H. Weber, and M. Mayor, *Proc. Natl. Acad. Sci. USA* **102**, 8815 (2005).
- ²² N. Ogawa, G. Mikaelian, and W. Ho, *Phys. Rev. Lett.* **98**, 166103 (2007).
- ²³ G. Schulze, K. J. Franke, A. Gagliardi, G. Romano, C. S. Lin, A. Da Rosa, T. A. Niehaus, T. Frauenheim, A. Di Carlo, A. Pecchia, and J. Pascual, *Phys. Rev. Lett.* **100**, 136801 (2008).
- ²⁴ F. Pump, R. Temirov, O. Neucheva, S. Soubatch, S. Tautz, M. Rohlfing, and G. Cuniberti, *Appl. Phys. A* **93**, 335 (2008).
- ²⁵ N. P. de Leon, W. Liang, Q. Gu, and H. Park, *Nano Lett.* **8**, 2963 (2008).
- ²⁶ E. A. Osorio, M. Ruben, J. S. Seldenthuis, J. M. Lehn, and H. S. J. van der Zant, *Small* **6**, 174 (2010).
- ²⁷ J. Hihath, C. Bruot, and N. Tao, *ACS Nano* **4**, 3823 (2010).
- ²⁸ C. A. Martin, J. M. van Ruitenbeek, and H. S. J. van de Zant, *Nanotechnology* **21**, 265201 (2010).
- ²⁹ W. Liang, M. Shores, M. Bockrath, J. Long, and H. Park, *Nature (London)* **417**, 725 (2002).
- ³⁰ J. Chen, M. Reed, A. Rawlett, and J. Tour, *Science* **286**, 1550 (1999).
- ³¹ J. Gaudio, L. J. Lauhon, and W. Ho, *Phys. Rev. Lett.* **85**, 1918 (2000).
- ³² A. Blum, J. Kushmerick, D. Long, C. Patterson, J. Jang, J. Henderson, Y. Yao, J. Tour, R. Shashidhar, and B. Ratna, *Nat. Mater.* **4**, 167 (2005).
- ³³ B.-Y. Choi, S.-J. Kahng, S. Kim, H. Kim, H. Kim, Y. Song, J. Ihm, and Y. Kuk, *Phys. Rev. Lett.* **96**, 156106 (2006).
- ³⁴ E. Lörtscher, J. W. Ciszek, J. Tour, and H. Riel, *Small* **2**, 973 (2006).
- ³⁵ B. Stipe, M. Rezai, and W. Ho, *Science* **280**, 1732 (1998).
- ³⁶ J. Kushmerick, J. Lazorcik, C. Patterson, R. Shashidhar, D. S. Seferos, and G. C. Bazan, *Nano Lett.* **4**, 639 (2004).
- ³⁷ A. Pasupathy, J. Park, C. Chang, A. Soldatov, S. Lebedkin, R. Bialczak, J. Grose, L. Donev, J. Sethna, D. Ralph, and P. McEuen, *Nano Lett.* **5**, 203 (2005).
- ³⁸ A. Pasupathy, J. Park, C. Chang, A. Soldatov, S. Lebedkin, R. Bialczak, J. Grose, L. Donev, J. Sethna, D. Ralph, and P. McEuen, *Nano Lett.* **5**, 203 (2005).
- ³⁹ S. Sapmaz, P. Jarillo-Herrero, Y. M. Blanter, C. Dekker, and H. S. van der Zant, *Phys. Rev. Lett.* **96**, 026801 (2006).
- ⁴⁰ W. H. A. Thijssen, D. Djukic, A. F. Otte, R. H. Bremmer, and J. M. van Ruitenbeek, *Phys.*

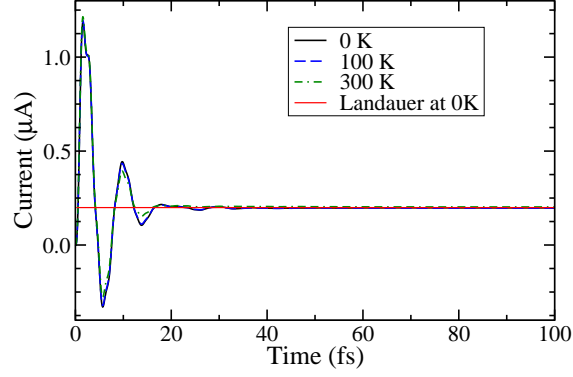
- Rev. Lett. **97**, 226806 (2006).
- ⁴¹ J. Parks, A. Champagne, G. Hutchison, S. Flores-Torres, H. Abruna, and D. Ralph, Phys. Rev. Lett. **99**, 026601 (2007).
- ⁴² T. Böhler, A. Edtbauer, and E. Scheer, Phys. Rev. B **76**, 125432 (2007).
- ⁴³ L. H. Yu, Z. K. Keane, J. W. Ciszek, L. Cheng, M. P. Stewart, J. M. Tour, and D. Natelson, Phys. Rev. Lett. **93**, 266802 (2004).
- ⁴⁴ A. K. Hüttel, B. Witkamp, M. Leijnse, M. R. Wegewijs, and H. S. J. van der Zant, Phys. Rev. Lett. **102**, 225501 (2009).
- ⁴⁵ S. Ballmann, W. Hieringer, D. Secker, Q. Zheng, J. A. Gladysz, A. Görling, and H. B. Weber, Chem. Phys. Chem. **11**, 2256 (2010).
- ⁴⁶ D. Secker, S. Wagner, S. Ballmann, R. Härtle, M. Thoss, and H. Weber, Phys. Rev. Lett. **106**, 136807 (2011).
- ⁴⁷ Z. Ioffe, T. Shamai, A. Ophir, G. Noy, I. Yutsis, K. Kfir, O. Cheshnovsky, and Y. Selzer, Nature Nanotech. **3**, 727 (2008).
- ⁴⁸ Z. Huang, B. Xu, Y. Chen, M. D. Ventra, and N. Tao, Nano Lett. **6**, 1240 (2006).
- ⁴⁹ D. R. Ward, N. J. Halas, J. W. Ciszek, J. M. Tour, Y. Wu, P. Nordlander, and D. Natelson, Nano Lett. **8**, 919 (2008).
- ⁵⁰ C. Benesch, M. Cizek, J. Klimes, I. Kondov, M. Thoss, and W. Domcke, J. Phys. Chem. C **112**, 9880 (2008).
- ⁵¹ H. Ness, S. Shevlin, and A. Fisher, Phys. Rev. B **63**, 125422 (2001).
- ⁵² M. Cizek, M. Thoss, and W. Domcke, Phys. Rev. B **70**, 125406 (2004).
- ⁵³ M. Cizek, M. Thoss, and W. Domcke, Czech. J. Phys. **55**, 189 (2005).
- ⁵⁴ M. Caspary-Toroker and U. Peskin, J. Chem. Phys. **127**, 154706 (2007).
- ⁵⁵ J. Bonca and S. Trugmann, Phys. Rev. Lett. **75**, 2566 (1995).
- ⁵⁶ N. A. Zimbovskaya and M. M. Kuklja, J. Chem. Phys. **131**, 114703 (2009).
- ⁵⁷ R. Jorn and T. Seidemann, J. Chem. Phys. **131**, 244114 (2009).
- ⁵⁸ A. Mitra, I. Aleiner, and A. J. Millis, Phys. Rev. B **69**, 245302 (2004).
- ⁵⁹ M. Galperin, M. Ratner, and A. Nitzan, Phys. Rev. B **73**, 045314 (2006).
- ⁶⁰ D. A. Ryndyk, M. Hartung, and G. Cuniberti, Phys. Rev. B **73**, 045420 (2006).
- ⁶¹ R. Härtle, C. Benesch, and M. Thoss, Phys. Rev. B **77**, 205314 (2008).
- ⁶² R. Härtle, C. Benesch, and M. Thoss, Phys. Rev. Lett. **102**, 146801 (2009).

- ⁶³ K. Flensberg, Phys. Rev. B **68**, 205323 (2003).
- ⁶⁴ M. Tahir and A. MacKinnon, Phys. Rev. B **77**, 224305 (2008).
- ⁶⁵ J. P. Bergfield and C. A. Stafford, Phys. Rev. B **79**, 245125 (2009).
- ⁶⁶ T. Frederiksen, M. Paulsson, M. Brandbyge, and A. Jauho, Phys. Rev. B **75**, 205413 (2007).
- ⁶⁷ V. May, Phys. Rev. B **66**, 245411 (2002).
- ⁶⁸ J. Lehmann, S. Kohler, V. May, and P. Hänggi, J. Chem. Phys. **121**, 2278 (2004).
- ⁶⁹ J. N. Pedersen and A. Wacker, Phys. Rev. B **72**, 195330 (2005).
- ⁷⁰ U. Harbola, M. Esposito, and S. Mukamel, Phys. Rev. B **74**, 235309 (2006).
- ⁷¹ A. Zazunov, D. Feinberg, and T. Martin, Phys. Rev. B **73**, 115405 (2006).
- ⁷² L. Siddiqui, A. W. Ghosh, and S. Datta, Phys. Rev. B **76**, 085433 (2007).
- ⁷³ C. Timm, Phys. Rev. B **77**, 195416 (2008).
- ⁷⁴ V. May and O. Kühn, Phys. Rev. B **77**, 115439 (2008).
- ⁷⁵ V. May and O. Kühn, Phys. Rev. B **77**, 115440 (2008).
- ⁷⁶ M. Leijnse and M. R. Wegewijs, Phys. Rev. B **78**, 235424 (2008).
- ⁷⁷ M. Esposito and M. Galperin, Phys. Rev. B **79**, 205303 (2009).
- ⁷⁸ R. Härtle and M. Thoss, Phys. Rev. B **83**, 115414 (2011).
- ⁷⁹ H. Wang and M. Thoss, J. Chem. Phys. **131**, 024114 (2009).
- ⁸⁰ L. Mühlbacher and E. Rabani, Phys. Rev. Lett. **100**, 176403 (2008).
- ⁸¹ S. Weiss, J. Eckel, M. Thorwart, and R. Egger, Phys. Rev. B **77**, 195316 (2008).
- ⁸² D. Segal, A.J.Millis, and D. Reichman, Phys. Rev. B **82**, 205323 (2010).
- ⁸³ P. Werner¹, T. Oka, and A. J. Millis, Phys. Rev. B **79**, 035320 (2009).
- ⁸⁴ M. Schiro and M. Fabrizio, Phys. Rev. B **79**, 153302 (2009).
- ⁸⁵ F. B. Anders, Phys. Rev. Lett. **101**, 066804 (2008).
- ⁸⁶ F. Heidrich-Meisner, A. Feiguin, and E. Dagotto, Phys. Rev. B **79**, 235336 (2009).
- ⁸⁷ J. Eckel, F. Heidrich-Meisner, S. Jakobs, M. Thorwart, M. Pletyukhov, and R. Egger, New. J. Phys. **12**, 043042 (2010).
- ⁸⁸ C. Benesch, M. Rode, M. Cizek, R. Härtle, O. Rubio-Pons, M. Thoss, and A. Sobolewski, J. Phys. Chem. C **112**, 9880 (2008).
- ⁸⁹ A. J. Leggett, S. Chakravarty, A. T. Dorsey, M. P. A. Fisher, A. Garg, and W. Zwerger, Rev. Mod. Phys. **59**(1), 1 (1987).
- ⁹⁰ U. Weiss, *Quantum Dissipative Systems* (World Scientific, Singapore, 1993).

- ⁹¹ H. Wang and M. Thoss, *J. Chem. Phys.* **119**(3), 1289 (2003).
- ⁹² A. Goldberg and B. W. Shore, *J. Phys. B* **11**, 3339 (1978).
- ⁹³ R. Kosloff and D. Kosloff, *J. Comput. Phys.* **63**, 363 (1986).
- ⁹⁴ D. Neuhauser and M. Baer, *J. Chem. Phys.* **90**, 4351 (1989).
- ⁹⁵ T. Seideman and W. H. Miller, *J. Chem. Phys.* **96**, 4412 (1991).
- ⁹⁶ H. Wang and M. Thoss, *Chem. Phys.* **370**, 78 (2010).
- ⁹⁷ J. Frenkel, *Wave Mechanics* (Clarendon Press, Oxford, 1934).
- ⁹⁸ M. Thoss and H. Wang, *Chem. Phys.* **322**(1-2), 210 (2006).
- ⁹⁹ H. Wang and M. Thoss, *J. Chem. Phys.* **124**(3), 034114 (2006).
- ¹⁰⁰ I. Kondov, H. Wang, and M. Thoss, *J. Phys. Chem. A* **110**(4), 1364 (2006).
- ¹⁰¹ H. Wang and M. Thoss, *J. Phys. Chem. A* **111**, 10369 (2007).
- ¹⁰² I. Kondov, M. Cizek, C. Benesch, H. Wang, and M. Thoss, *J. Phys. Chem. C* **111**(32), 11970 (2007).
- ¹⁰³ M. Thoss, I. Kondov, and H. Wang, *Phys. Rev. B* **76**, 153313 (2007).
- ¹⁰⁴ H. Wang and M. Thoss, *Chem. Phys.* **347**, 139 (2008).
- ¹⁰⁵ H. Wang and M. Thoss, *New J. Phys.* **10**, 115005 (2008).
- ¹⁰⁶ D. Egorova, M. F. Gelin, M. Thoss, H. Wang, and W. Domcke, *J. Chem. Phys.* **129**, 214303 (2008).
- ¹⁰⁷ K. A. Velizhanin and H. Wang, *J. Chem. Phys.* **131**, 094109 (2009).
- ¹⁰⁸ O. Vendrell and H.-D. Meyer, *J. Chem. Phys.* **134**, 2011 (044135).
- ¹⁰⁹ K. A. Velizhanin, H. Wang, and M. Thoss, *Chem. Phys. Lett.* **460**, 325 (2008).
- ¹¹⁰ H. Wang, D. Skinner, and M. Thoss, *J. Chem. Phys.* **125**, 174502 (2006).
- ¹¹¹ I. R. Craig, M. Thoss, and H. Wang, *J. Chem. Phys.* **127**, 144503 (2007).
- ¹¹² U. Manthe, *J. Chem. Phys.* **128**, 164116 (2008).
- ¹¹³ U. Manthe, *J. Chem. Phys.* **130**, 054109 (2009).
- ¹¹⁴ T. Kato and H. Kono, *Chem. Phys. Lett.* **392**, 533 (2004).
- ¹¹⁵ J. Caillat, J. Zanghellini, M. Kitzler, O. Koch, W. Kreuzer, and A. Scrinzi, *Phys. Rev. A* **71**, 012712 (2005).
- ¹¹⁶ M. Nest, T. Klamroth, and P. Saalfrank, *J. Chem. Phys.* **122**, 124102 (2005).
- ¹¹⁷ O. E. Alon, A. I. Streltsov, and L. S. Cederbaum, *Phys. Rev. A* **77**, 033613 (2008).
- ¹¹⁸ O. Alon, A. Streltsov, and L. Cederbaum, *J. Chem. Phys.* **127**, 154103 (2007).

- ¹¹⁹ W. Greiner, *Quantum Mechanics, Special Chapters* (Springer, Berlin, 1998).
- ¹²⁰ A. Fetter and J. Walecka, *Quantum Theory of Many-Particle Systems* (McGraw Hill, New York, 1971).
- ¹²¹ G. Mahan, *Many-Particle Physics* (Plenum Press, 1981).
- ¹²² R. Landauer, IBM J. Res. Dev. **1**, 223 (1957).
- ¹²³ S. Datta, *Electric Transport in Mesoscopic Systems* (Cambridge University Press, Cambridge, 1995).
- ¹²⁴ M. Galperin, M. Ratner, and A. Nitzan, Nano Lett. **5**, 125 (2005).
- ¹²⁵ A. Alexandrov and A. Bratkovsky, J. Phys.: Condens. Matter **19**, 255203 (2007).
- ¹²⁶ M. Galperin, M. Ratner, and A. Nitzan, J. Phys.: Condens. Matter **20**, 374107 (2008).
- ¹²⁷ D. A. Ryndyk, P. D'Amico, G. Cuniberti, and K. Richter, Phys. Rev. B **78**, 085409 (2008).
- ¹²⁸ P. D'Amico, D. A. Ryndyk, G. Cuniberti, and K. Richter, New J. Phys. **10**, 085002 (2008).
- ¹²⁹ R.-P. Riwar and T. Schmidt, Phys. Rev. B **80**, 125109 (2009).
- ¹³⁰ F. Albrecht, A. Komnik, M. Thoss, L. Mühlbacher, and H. Wang, to be published.
- ¹³¹ E. Weig, R. Blick, T. Brandes, J. Kirschbaum, W. Wegscheider, M. Bichler, and J. P. Kotthaus, Phys. Rev. Lett. **92**, 046804 (2004).
- ¹³² R. Volkovich, R. Härtle, M. Thoss, and U. Peskin, Phys. Chem. Chem. Phys. **13**, 14333 (2011).
- ¹³³ J. Koch and F. von Oppen, Phys. Rev. Lett. **94**, 206804 (2005).
- ¹³⁴ J. Koch and F. von Oppen, Phys. Rev. B **74**, 205438 (2006).
- ¹³⁵ R. Leturcq, C. Stampfer, K. Inderbitzin, L. Durrer, C. Hierold, E. Mariani, M. Schultz, F. von Oppen, and K. Ensslin, Nature Physics **5**, 327 (2009).

(a)



(b)

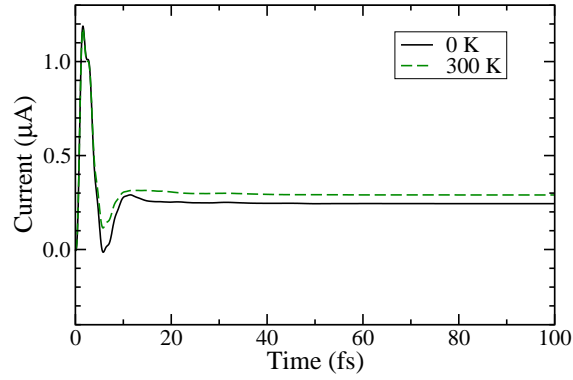


FIG. 1: Time-dependent current $I(t)$ at different temperatures. The parameters are: $\alpha_e = 0.2\text{eV}$, $\beta_e = 1\text{eV}$, $E_d - E_f = 0.5\text{eV}$, and $V = 0.2\text{V}$. Results in panel (a) have been obtained without coupling to the vibrations ($\lambda = 0$). In panel (b) couplings to an Ohmic bath of vibrational modes with parameters are $\lambda = 2000\text{cm}^{-1}$ and $\omega_c = 500\text{cm}^{-1}$ is included. The red line in panel (a) shows the current for a purely electronic model ($\lambda = 0$) as obtained from Landauer theory

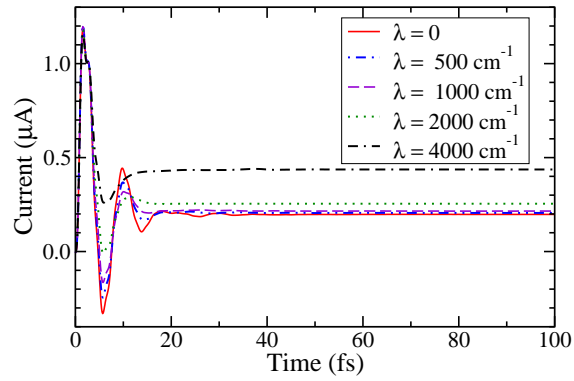


FIG. 2: Time-dependent current $I(t)$ for different coupling strengths to the vibrational bath as specified by the reorganization energy λ at temperature $T = 0$ and bias voltage $V = 0.2\text{V}$. All other parameters are the same as in Fig. 1(b).

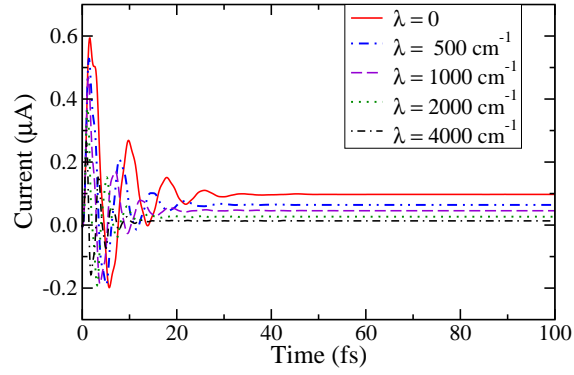
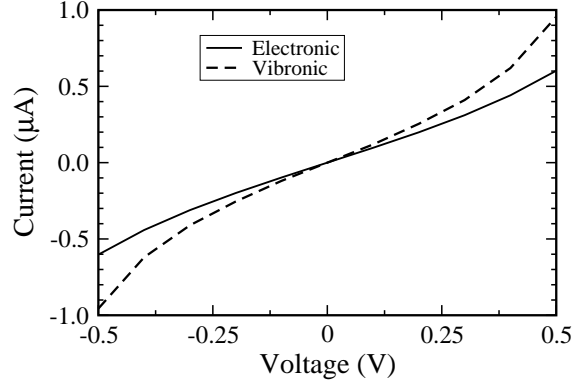


FIG. 3: Time-dependent current $I(t)$ for different coupling strengths to the vibrational bath as specified by the reorganization energy λ at temperature $T = 0$ and bias voltage $V = 0.1\text{V}$. Except for $E_d - E_f = -0.5\text{eV}$, all other parameters are the same as in Fig. 1(b).

(a)



(b)

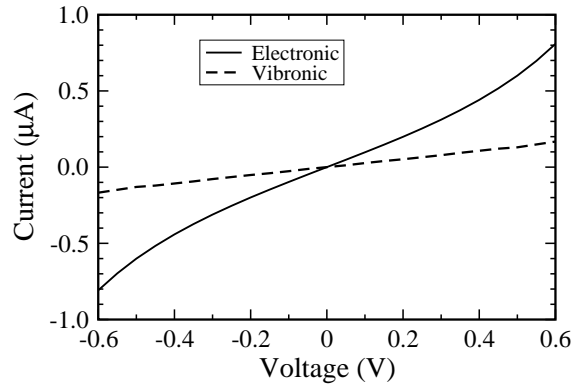
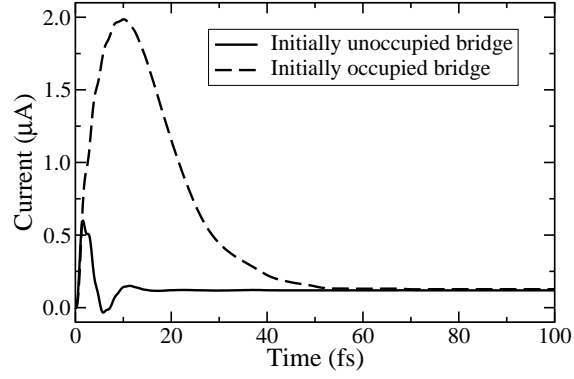


FIG. 4: Current-voltage characteristics for vibrational coupled electron transport. The parameters for the electronic lead states are $\alpha_e = 0.2\text{eV}$ and $\beta_e = 1\text{eV}$. The vibrational parameters are $\lambda = 2000\text{cm}^{-1}$ and $\omega_c = 500\text{cm}^{-1}$. The energy of the bridge state is located at: (a) $E_d - E_f = 0.5\text{eV}$, (b) $E_d - E_f = -0.5\text{eV}$. The dashed lines depict the current for a purely electronic model ($\lambda = 0$)

(a)



(b)

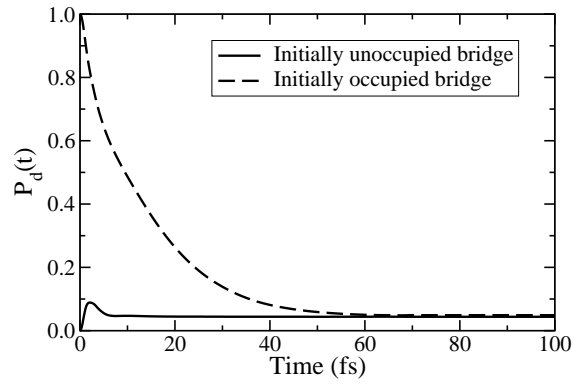


FIG. 5: Dependence of the time-dependent electric current (a) and the population of the bridge state (b) on the initial state. The electronic parameters are $\alpha_e = 0.2\text{eV}$, $\beta_e = 1\text{eV}$, $E_d - E_f = 0.5\text{eV}$, and $V = 0.1\text{V}$. The vibrational parameters are $\lambda = 2000\text{cm}^{-1}$ and $\omega_c = 500\text{cm}^{-1}$.

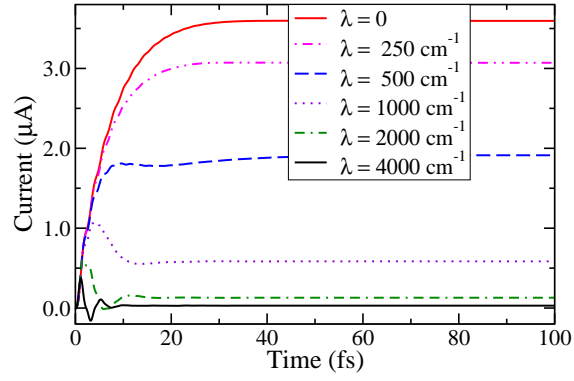


FIG. 6: Time-dependent current $I(t)$ in the phonon-blockade regime for different coupling strengths to the vibrational bath as specified by the reorganization energy λ . The electronic parameters are $\alpha_e = 0.2\text{eV}$, $\beta_e = 1\text{eV}$, $E_d - E_f = 0$, and $V = 0.1\text{V}$. The characteristic frequency of the vibrational bath is $\omega_c = 500\text{cm}^{-1}$.

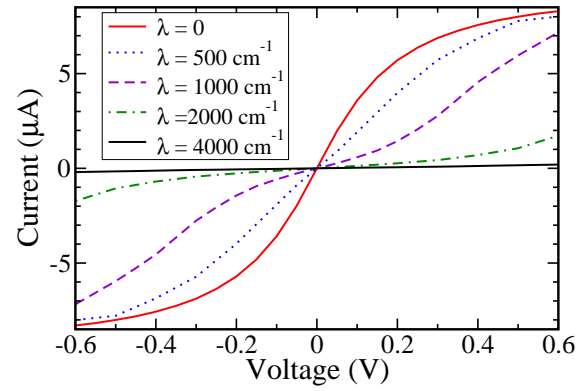


FIG. 7: Dependence of the current-voltage characteristics in the phonon-blockade regime on the electronic-vibrational coupling strength. The electronic parameters are the same as in Fig. 6, with $\omega_c = 500\text{cm}^{-1}$.

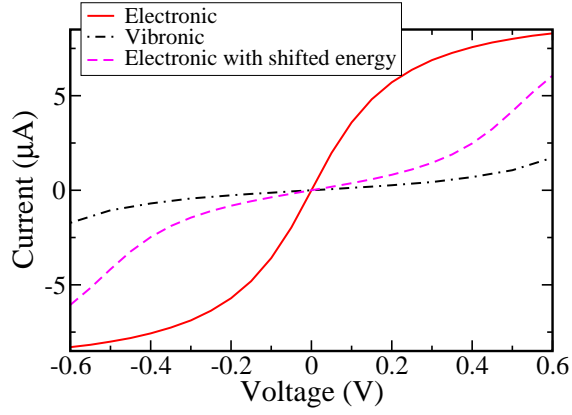
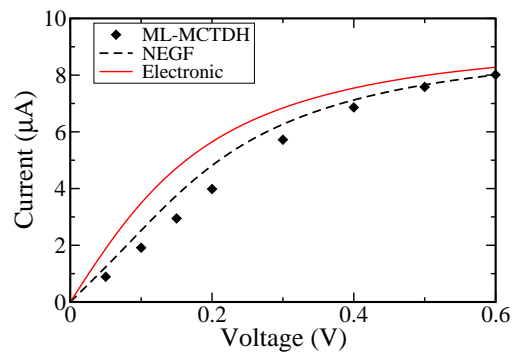
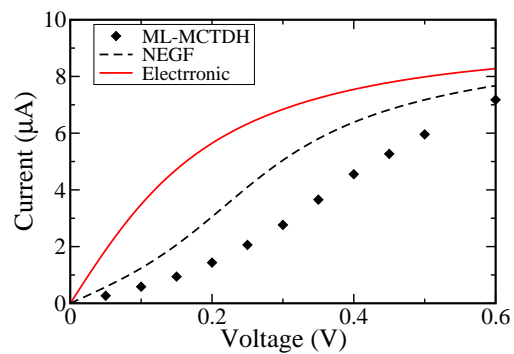


FIG. 8: Current-voltage characteristics for vibrationally coupled electron transport in the phonon-blockade regime. The electronic parameters are the same as in Fig. 6. The vibrational parameters are $\lambda = 2000\text{cm}^{-1}$ and $\omega_c = 500\text{cm}^{-1}$. Shown are results of a purely electronic model employing the bare (full line) and the polaron-shifted (dashed line) energy of the discrete state, respectively, as well as results of a full vibrationally-coupled many-body ML-MCTDH-SQR calculation (dashed-dotted line).

(a)



(b)



(c)

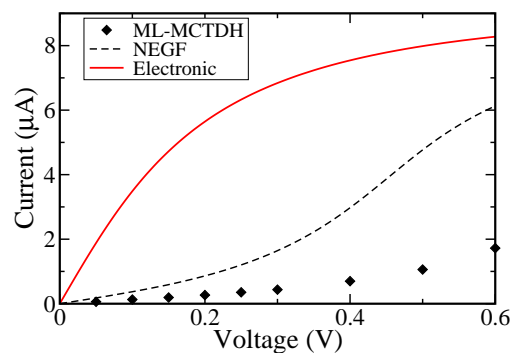


FIG. 9: Comparison of results obtain with NEGF theory (dashed lines) and the ML-MCTDH-SQR method (diamonds) for vibronic coupling parameters $\lambda = 500\text{cm}^{-1}$ (a), $\lambda = 1000\text{cm}^{-1}$ (b), and $\lambda = 2000\text{cm}^{-1}$ (c). All other parameters are the same as in Fig. 6. In addition, results for a purely electronic model are shown (full lines).

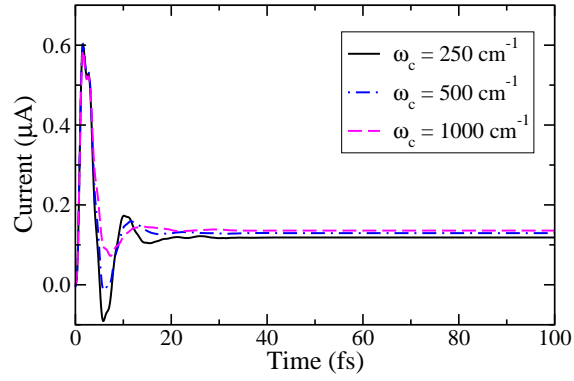
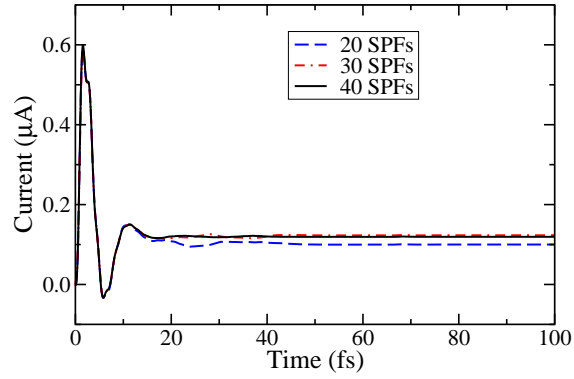
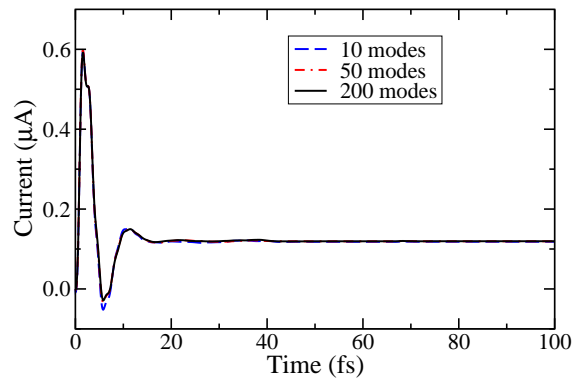


FIG. 10: Dependence of the time-dependent current $I(t)$ in the phonon-blockade regime on the characteristic frequency of the vibrational bath. The electronic parameters are $\alpha_e = 0.2\text{eV}$, $\beta_e = 1\text{eV}$, $E_d - E_f = 0$, and $V = 0.1\text{V}$. The reorganization energy is $\lambda = 2000\text{cm}^{-1}$.

(a)



(b)



(c)

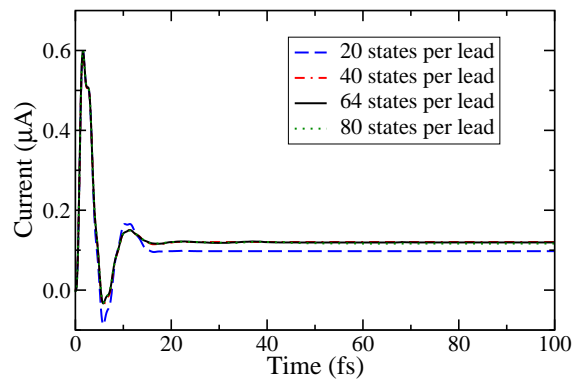


FIG. 11: Time-dependent current $I(t)$ for the parameter set of $\alpha_e = 0.2\text{eV}$, $\beta_e = 1\text{eV}$, $E_d - E_f = 0.5\text{eV}$, and $V = 0.1\text{V}$. Convergence is shown with respect to: (a) the number of SPFs for the electronic SPs; (b) the number of bath modes; (c) the number of electronic states for each lead. Other variational parameters are described in the text.